Synthesis of Palladium and Platinum Nanoclusters within Microphase-Separated Diblock Copolymers

Y. Ng Cheong Chan,[†] G. S. W. Craig,[‡] R. R. Schrock,*[,†] and R. E. Cohen[‡]

Departments of Chemistry and Chemical Engineering, Massachusetts Institute of Technology, Cambridge, Massachusetts 02139

Received February 25, 1992. Revised Manuscript Received April 6, 1992

Small palladium and platinum clusters have been synthesized within a purely hydrocarbon polymer matrix. The procedure consists of ring-opening metathesis polymerization of norbornene-derived organometallic complexes, $Pd(Cp^N)(PA)$ and $Pt(Cp^N)Me_3$ (Cp^N = *endo*-2-(cyclopentadienylmethyl)norborn-5-ene and PA = η^3-1-phenylallyl), using W or Mo alkylidene initiators, followed by static casting of films and subsequent reduction of the organometallic complexes under mild conditions using molecular hydrogen. Diblock copolymers of the organometallic monomers and methyltetracyclododecene (MTD) also were prepared. Under suitable conditions these copolymers underwent microphase separation, resulting in lamellar, cylindrical, and spherical morphologies. The metal clusters formed in the copolymer films exhibiting lamellar and cylindrical morphologies were predominantly within the original metal-containing microdomains, had a narrow size distribution compared to the clusters formed in the homopolymer films, and were less than 100 Å in diameter.

Introduction

Metal nanoclusters are of considerable interest because they can exhibit physical and chemical properties that differ from those of bulk metal. In some cases, the unique properties of these small metal particles (~10–100 Å in diameter) can be attributed to quantum size effects or to the increased ratio of surface to bulk atoms.[1-5] There also has been extensive research on the catalytic properties of these clusters.[6-10] Flytzanis and co-workers studied the nonlinear optical properties of gold and silver clusters in a dielectric medium and predicted that the third-order susceptibility of the clusters would vary as the inverse third power of their radii.[11] In these cases, a small cluster size and narrow size distribution are desirable. In other cases the uniform dispersion of the clusters within the matrix is necessary. For example, a dispersion of conductive metal particles in a nonconductive material should result in a composite material that has a very large dielectric constant.[12] Therefore the ability to control the size, the size distribution, and the spatial distribution of clusters throughout a matrix is highly desirable.

Methods of synthesizing macroscopic quantities of a composite material consisting of uniformly sized metal nanoclusters homogeneously dispersed in a stabilizing, nonconductive medium to give a processable solid material are scarce.[13] Polymer/metal cluster composites have been obtained by methods that involve evaporation of metal atoms into polymer solutions[7,14-17] or addition of polymers to aqueous colloidal solutions[18,19] of reduced metal salts followed by evaporation of the solvent. Metal clusters also have been synthesized and studied within an SiO_2 matrix by sol–gel processes.[20-23] In many cases large sections of the matrix material contained no clusters, or small clusters aggregated into larger clusters; it was not possible to obtain uniformly dispersed clusters with a narrow size distribution.

The purpose of this research is to explore the possibility of synthesizing metal clusters that are less than 100 Å in diameter, that have a narrow size distribution, and that are dispersed evenly throughout a nonconductive polymer matrix. This paper presents two routes to the formation of such composite materials, namely, the reduction of the metal complexes and aggregation of the metal atoms in the solid state either in an organometallic homopolymer or in the organometallic block of a microphase-separated diblock copolymer. Two organometallic, norbornene-derived monomers, $Pd(Cp^N)(PA)$ and $Pt(Cp^N)Me_3$ (Cp^N = *endo*-2-(cyclopentadienylmethyl)norborn-5-ene and PA = η^3-1-phenylallyl), shown in Scheme I, were synthesized in order to incorporate the respective metal atoms into the polymer system. These monomers were polymerized via living ring-opening metathesis polymerization (ROMP[24]) initiated by well-defined W or Mo alkylidene complexes[25,26] to

[†] Department of Chemistry.
[‡] Department of Chemical Engineering.

(1) Halperin, W. P. *Rev. Mod. Phys.* **1986**, *58*, 533.
(2) Steigerwald, M. L.; Brus, L. E. *Annu. Rev. Mater. Sci.* **1989**, *19*, 471.
(3) Bond, G. C. *Surf. Sci.* **1985**, *156*, 966.
(4) Stucky, G. D.; MacDougall, J. E. *Science* **1990**, *247*, 669.
(5) Wang, Y. *Acc. Chem. Res.* **1991**, *24*, 133.
(6) Yermakov, Y. I. *J. Mol. Catal.* **1983**, *21*, 35.
(7) Klabunde, K. J.; Habdas, J.; Cardenas-Trivino, G. *Chem. Mater.* **1989**, *1*, 481.
(8) Lewis, L. N.; Lewis, N. *Chem. Mater.* **1989**, *1*, 106.
(9) Hable, C. T.; Wrighton, M. S. *Langmuir* **1991**, *7*, 1305.
(10) Pocard, N. L.; Alsmeyer, D. C.; McCreery, R. L.; Neenan, T. X.; Callstrom, M. R. *J. Am. Chem. Soc.* **1992**, *114*, 769.
(11) Hache, F.; Ricard, D.; Flytzanis, C. *J. Opt. Soc. Am. B* **1986**, *3*, 1647.
(12) Kirkpatrick, S. *Rev. Mod. Phys.* **1973**, *45*, 574.
(13) Andres, R. P.; Averback, R. S.; Brown, W. L.; Brus, L. E.; Godard III, W. A.; Kaldor, A.; Louie, S. G.; Moscovits, M.; Peercy, P. S.; Riley, S. J.; Siegel, R. w.; Spaepen, F.; Wang, Y. *J. Mater. Res.* **1989**, *4*, 704.
(14) Andres, M. P.; Ozin, G. A. *Chem. Mater.* **1989**, *1*, 174.
(15) Bradley, J. S.; Hill, E.; Leonowicz, M. E.; Witzke, H. *J. Mol. Catal.* **1987**, *41*, 59.
(16) Noguchi, T.; Gotoh, K.; Yamaguchi, Y.; Deki, S. *J. Mater. Sci. Lett.* **1991**, *10*, 447.
(17) Perrin, J.; Despax, B.; Kay, E. *Phys. Rev. B.* **1985**, *32*, 719.
(18) Van Rheenen, P.; McKelvy, M.; Marzke, R.; Glaunsinger, W. S. *Inorg. Synth.* **1986**, 238.
(19) Nakao, Y.; Kaeriyama, K. *Bull. Chem. Soc. Jpn.* **1987**, *60*, 4465.
(20) Breitscheidel, B.; Zieder, J.; Schubert, U. *Chem. Mater.* **1991**, *3*, 559.
(21) Tour, J. M.; Pendalwar, L. S.; Copper, J. P. *Chem. Mater.* **1990**, *2*, 647.
(22) Kaiser, W. J.; Logothetis, E. M.; Wenger, L. E. *J. Phys. C* **1985**, *18*, L837.
(23) Lee, S.-I.; Noh, T. W.; Gaines, J. R.; Ko, V.-H.; Kreider, E. R. *Phys. Rev. B* **1988**, *37*, 2918.
(24) Grubbs, R. H.; Tumas, W. *Science* **1989**, *243*, 907.

0897-4756/92/2804-0885$03.00/0

give polymers in which a metal complex is covalently attached to each repeat unit. The diblock copolymers were prepared in an analogous fashion by sequential polymerization of methyltetracyclododecene (MTD) and one of the organometallic monomers. Polymer films were static cast from solution. The metal complexes were then reduced by treatment with molecular hydrogen and, in the case of the platinum compound, also by UV light. Continued treatment with hydrogen accompanied by mild heating led to aggregation of the metal atoms and formation of clusters.

It is well-known that diblock copolymers can undergo microphase separation, forming lamellar, cylindrical, spherical morphologies,[27-34] and the ordered bicontinuous double diamond morphology.[35,36] Much of this work has been concerned with wholly organic block copolymers such as polystyrene/polybutadiene. The samples prepared here displayed the three primary morphologies. In the case of the diblock copolymers, the goal was to utilize the microphase-separated morphology of the bulk copolymer as an additional kinetic barrier to the aggregation of small clusters into larger particles. The morphology of the polymers (before and after treatment, as appropriate) and the metal clusters were characterized by transmission electron microscopy (TEM), electron diffraction (ED), small-angle X-ray scattering with a two-dimensional detector (SAXS), and wide-angle X-ray scattering (WAXS).

There are additional advantages to the organometallic diblock approach. First, the type of morphology and the domain size (and in our case the metal content) can be controlled by adjusting the molecular weight and the composition of the diblock. Furthermore, the metal complexes are connected to each monomer in the polymer and consequently are initially distributed homogeneously within the microdomains. Finally, the thermally induced aggregation can occur at a temperature far below the T_g (~210 °C) of the polyMTD[37] host polymer matrix, providing an additional degree of kinetic restraint of cluster aggregation.

In a previous communication[38] we reported the synthesis of diblock copolymers in which silver and gold complexes were attached to one of the blocks in a ROMP block copolymer via coordination to phosphine centers; the block copolymers exhibited microphase separation, and thermal treatment of the polymer films resulted in the formation of silver and gold clusters less than 100 Å in diameter that resided mostly within the original metal-complex containing microdomains. The synthesis of metal sulfide semiconductor clusters within diblock copolymer microdomains has also been reported recently.[39-43]

Experimental Section

General Methods. All experiments were performed under a nitrogen atmosphere in a Vacuum Atmospheres drybox or by using standard Schlenk/vacuum line techniques. THF and benzene were distilled from purple benzophenone ketyl under nitrogen. Pentane was washed with 5% nitric acid in sulfuric acid, stored over calcium chloride, and then distilled from sodium benzophenone ketyl under nitrogen. Toluene for polymerization was distilled over sodium and then stored over sodium/potassium alloy under nitrogen and filtered prior to use. MTD was purified by vacuum distillation over sodium. $Mo(CHCMe_2Ph)(NAr)(O\text{-}t\text{-}Bu)_2$,[44] $W(CH\text{-}t\text{-}Bu)(NAr)(O\text{-}t\text{-}Bu)_2$ (Ar = 2,6-diisopropylphenyl),[45] $[Pd(PA)Cl]_2$,[46] and $[PtMe_3I]_4$[47] were synthesized according to literature procedures. HCp^N was synthesized at low temperature from an $AlEt_2Cl$-catalyzed Diels–Alder reaction between cyclopentadiene and methyl acrylate,[48] followed by reduction to *endo*-2-(hydroxymethyl)norborn-5-ene using $LiAlH_4$, tosylation, and treatment with NaCp. $Li(Cp^N)$ is then obtained by reaction of HCp^N with Li-*n*-Bu in pentane.[49]

^1H NMR spectra were recorded at 300 MHz. Chemical shifts are listed in parts per million downfield from TMS. Gel permeation chromatographic (GPC) analysis was carried out at room temperature employing a Rheodyne Model 7125 sample injector, a Kratos Spectroflow 400 pump, Shodex KF-802.5, 803, 804, 805, and 800P columns, a Knauer differential refractometer, and a Spectroflow 757 absorbance detector on samples 0.1–0.3 % w/v in tetrahydrofuran which were filtered through a Millex-SR 0.5-μm filter to remove particulates. The GPC columns were calibrated versus commercially available polystyrene standards (Polymer Laboratories Ltd.) ranging from 1206 to 1.03×10^6 MW. A Perkin-Elmer DSC-7 differential scanning calorimeter was used to determine the thermal transitions of the organometallic homopolymers. The DSC was operated at a scanning rate of 20 °C/min.

$Pd(Cp^N)(PA)$. A solution of $LiCp^N$ (518 mg, 2.91 mmol) in 10 mL of THF at −30 °C was added dropwise to a stirred suspension of $[Pd(PA)Cl]_2$ (753 mg, 1.455 mmol) in 20 mL of THF/C_6H_6 (1/1, v/v) over 15 min. The deep red solution was then allowed to warm to room temperature and was stirred for 3 h. The solvent was removed in vacuo, and the residue was extracted with 20 mL of pentane to remove LiCl. Cooling to −30 °C gave 960 mg (84%) of purple red crystals in three crops: ^1H NMR (C_6H_6) δ 7.25–6.97 (m, 5 H, Ph), 6.05 (m, 1 H, olefin), 5.89 (m, 1 H, olefin), 5.72 (br s, 2 H, Cp), 5.63 (m, 1 H, Cp), 5.40 (br m, 1 H, Cp), 5.22 (m, 1 H, allyl), 3.81 (dd, 1 H, allyl), 3.37 (d, 1 H, allyl), 2.68 (br s, 1 H, bridgehead), 2.63 (br s, 1 H, bridgehead), 2.24 (d, 1 H, allyl), 2.03 (m, 1 H, exo methine), 1.80–1.65 (m, 3 H, 1 *exo*-CH_2, 2 $CpCH_2$), 1.44 (dm, 1 H, $C(7)H_2$), 1.08 (d, 1 H, $C(7)H_2$), 0.53 (ddd, 1 H, endo CH_2). Anal. Calcd for $PdC_{22}H_{24}$: C, 67.14; H, 6.48. Found: C, 66.93; H, 6.13.

$Pt(Cp^N)Me_3$. A solution of $LiCp^N$ (276 mg, 1.55 mmol) in 10 mL of THF was added dropwise to a solution of $[PtMe_3I]_4$ (541 mg, 1.47 mmol of Pt) in 15 mL of benzene at room temperature, and the mixture was stirred overnight. The colorless solution was evaporated to dryness and extracted three times with 20 mL of pentane. The volume of the solution was reduced to about 5 mL, and the solution was then filtered through 5 cm of dry neutral

(25) Schrock, R. R. *Acc. Chem. Res.* **1990**, *23*, 158.
(26) Wu, Z.; Wheeler, D. R.; Grubbs, R. H. *J. Am. Chem. Soc.* **1992**, *114*, 146.
(27) Bates, F. S. *Science* **1991**, *251*, 898.
(28) Quirk, P. R.; Kinning, D. J.; Fetters, L. J. In *Comprehensive Polymer Science*; Allen, G.; Bevington, J. C.; Aggarval, S. L., Eds.; Pergamon Press: New York, 1989; Vol. 7, p 1.
(29) Liebler, L. *Macromolecules* **1980**, *13*, 1602.
(30) Helfand, E.; Wasserman, Z. R. *Macromolecules* **1976**, *9*, 879.
(31) Helfand, E.; Wasserman, Z. R. *Macromolecules* **1978**, *11*, 960.
(32) Helfand, E.; Wasserman, Z. R. *Macromolecules* **1980**, *13*, 994.
(33) Hashimoto, T.; Tanaka, H.; Hasegawa, H. *Macromolecules* **1985**, *18*, 1864.
(34) Hadziioannou, G.; Skoulios, A. *Macromolecules* **1982**, *15*, 258.
(35) Hasegawa, H.; Tanaka, H.; Yamasaki, K.; Hashimoto, T. *Macromolecules* **1987**, *20*, 1651.
(36) Herman, D. S.; Kinning, D. J.; Thomas, E. L.; Fetters, L. J. *Macromolecules* **1987**, *20*, 2940.
(37) Schneider, W., US Patent 4,320,239, 1982.
(38) Ng Cheong Chan, Y.; Schrock, R. R.; Cohen, R. E. *Chem. Mater.* **1992**, *4*, 24.
(39) Sankaran, V.; Cummins, C. C.; Schrock, R. R.; Cohen, R. E.; Silbey, R. J. *J. Am. Chem. Soc.* **1990**, *112*, 6858.
(40) Sankaran, V.; Cohen, R. E.; Cummins, C. C.; Schrock, R. R. *Macromolecules* **1991**, *24*, 6664.
(41) Cummins, C. C.; Beachy, M. D.; Schrock, R. R.; Vale, M. G.; Sankaran, V.; Cohen, R. E. *Chem. Mater.* **1991**, *3*, 1153.
(42) Cummins, C. C.; Schrock, R. R.; Cohen, R. E. *Chem. Mater.* **1992**, *4*, 27.
(43) Moller, M. *Synth. Met.* **1991**, 41-43, 1159.
(44) Schrock, R. R.; Murdzek, J. S.; Bazan, G. C.; Robbins, J.; DiMare, M.; O'Regan, M. *J. Am. Chem. Soc.* **1990**, *112*, 3875.
(45) Schrock, R. R.; DePue, R. T.; Feldman, J.; Yap, K. B.; Yang, D. C.; Davis, W. M.; Park, L. Y.; DiMare, M.; Schofield, M.; Anhaus, J.; Walborsky, E.; Evitt, E.; Krüger, C.; Betz, P. *Organometallics* **1990**, *9*, 2262.
(46) Sakakibara, M.; Takahashi, Y.; Sakai, S.; Ishii, Y. *J. Chem. Soc., Chem. Commun.* **1969**, 396.
(47) Baldwin, J. C.; Kaska, W. C. *Inorg. Chem.* **1975**, *14*, 2020.
(48) Furuta, K.; Iwanaga, K.; Yamamoto, H. *Tetrahedron Lett.* **1986**, *27*, 4507.
(49) Cummins, C. C., unpublished results.

alumina. The column was washed with 10 mL of pentane, and the combined filtrates were evaporated to yield a colorless viscous liquid, 483 mg (80%). An impurity having a proton NMR resonance at 5.95 ppm was sometimes observed (<5%). It did not appear to affect polymerizations: ^{1}H NMR (C_6D_6) δ 6.05 (dd, 1 H, olefin), 5.85 (dd, 1 H, olefin), 5.16 (m, 2 H, Cp), 4.97 (m, 2 H, Cp), 2.61 (br s, 1 H, bridgehead), 2.58 (br s, 1 H, bridgehead), 1.97 (m, 1 H, exo methine), 1.91 (s, 1 H, $CpCH_2$), 1.89 (d, 1 H, $CpCH_2$), 1.66 (m, 1 H, *exo*-CH_2), 1.42 (dm, 1 H, C(7)H_2), 1.15 (s, 9 H, Me_3, satellites due to ^{195}Pt (spin $^1/_2$, 33.8%), $^2J_{HPt}$ = 82 Hz). Anal. Calcd for $PtC_{16}H_{24}$: C, 46.71; H, 5.88. Found: C, 47.26; H, 6.14.

General Procedure for Polymer Synthesis. The synthesis of the copolymer L, the $[Pd(Cp^N)(PA)]_{50}[MTD]_{113}$ diblock copolymer (see Table I), is given as an example. (In this paper, the numerical subscripts refer to the number of equivalents of each monomer that are sequentially added to 1 equiv of alkylidene initiator. Previous studies with the metal alkylidene initiators have shown that in many cases the number of equivalents added approximately equal the actual degree of polymerization of the individual blocks.[25]) A solution of $Mo(CHCMe_2Ph)(NAr)(O\text{-}t\text{-}Bu)_2$ (27.5 mg, 0.039 mmol) in 1 g of toluene was added all at once to a rapidly stirred solution of MTD (1.00 g, 5.738 mmol) in 26 g of toluene. After 15 min, 7 g of the solution was removed and capped with 20 mg of pivaldehyde (reaction time 30 min). $Pd(Cp^N)(PA)$ (750 mg, 1.90 mmol) in 10 g of toluene was added to the other part of the solution, and the mixture was stirred for 15 min and then quenched with 20 mg of pivaldehyde. The polyMTD homopolymer was precipitated in 100 mL of methanol and dried under vacuum overnight, yielding 248 mg (99%). The diblock copolymer was precipitated from 300 mL of stirred pentane. The precipitated polymer was collected by filtration, washed twice with 100 mL of pentane, and then dried under vacuum for 48 h; yield 1495 mg (100%). NMR analysis of the diblock showed the ratio of $Pd(Cp^N)(PA)$ to MTD to be 0.48 (calcd 0.50).

Microphase-separated copolymer films were static cast by dissolving 150 mg of the diblock in 6 g of benzene and then placing the solution in a polyethylene vial (diameter = 1 cm) in a glovebox under nitrogen. The benzene was allowed to evaporate slowly over 5–8 days. The dark red film thus obtained was then placed under high vacuum for at least 24 h prior to analysis.

Reduction of the Metal-Containing Polymers. The Pd-containing films were reduced in a stainless steel reactor or a Fischer-Porter bottle under a hydrogen pressure of 5 bar at 100 °C for several days. The Pt-containing films were reduced by first exposing them to medium-intensity UV light (Oriel Model 66002 mercury arc lamp) for 24 h and then treating them with hydrogens as for the Pd-containing films.

Morphological Characterization. TEM was performed on a JEOL 200 CX operated at 200 kV. Ultrathin samples for TEM were microtomed at room temperature with a LKB Ultratome III Model 8800 and deposited onto a copper grid. The films were microtomed to give thicknesses of 300–400 Å (before reduction of the metal complex) and 50–100 Å (after reduction of the bulk sample). Unless otherwise specified, the as-cast films were microtomed without encapsulation in epoxy. It also was possible to reduce the complex to form clusters in a microtomed section. However, the work reported here focuses on cluster formation in bulk samples.

SAXS and WAXS studies were performed on bulk samples. A Rigaku rotating Cu anode X-ray source (λ = 1.54 Å) was employed throughout the SAXS and WAXS studies. For SAXS, the Cu Kα line generated at 40 kV and 30 mA was focused and aligned with a Charles Supper double-mirror system. Scattering intensities were measured on a Nicolet two-dimensional area detector. The sample-to-detector distance was either 1.00 or 2.54 m. A helium-filled beam-line tube was employed to reduce random atmospheric scattering. For each sample, a set of scattering data with no sample present was subtracted from the raw scattering data to correct for sample absorption, background scattering, and detector inhomogeneities.

For WAXS studies, the Cu Kα line generated at 50 kV and 60 mA was filtered using electronic filtering and a thin Ni filter. The X-ray diffractometer and pole figure attachment were controlled on-line by means of a MicroVAX computer running under DMAXB Rigaku-USA software. The slit system allowed for the collection of the diffracted beam with a divergence angle of less than 0.2°. All the 2θ diffraction data were collected in transmission mode stepwise from 10° to 75° with a collection time of 4.0 s for each 0.05° step. Scherrer's formula was applied to each of the crystalline peaks in the WAXS profile to estimate the crystal sizes of the metal clusters.[50]

Scheme I

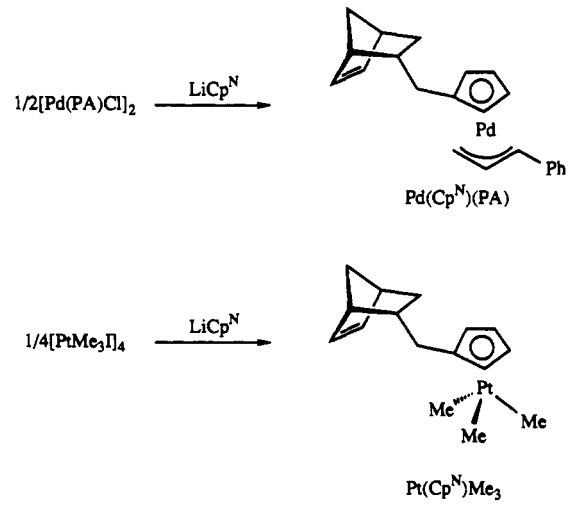

Morphological Modeling of SAXS Profiles. The radially averaged X-ray scattering profiles of the films containing spherical morphologies or metal clusters were modeled as in previous work on organic or organometallic block copolymers,[40,50,51] assuming a random distribution of spheres in the bulk matrix. Two scattering mechanisms were incorporated in the model: the interparticle interference and intraparticle scattering. Following the method described by Kinning and Thomas,[52] we used the Percus–Yevick[53] correlation function developed by Wertheim[54] and Thiele[55] for the interparticle scattering, while the intraparticle scattering was modeled with the single-particle form factor described by the Bessel function $J_{3/2}$.

Results

Monomer Synthesis and Properties. $Pd(Cp^N)(PA)$ and $Pt(Cp^N)Me_3$ are obtained in good yield by treating $[Pd(PA)Cl]_2$ and $[Pt(Me_3)I]_4$ respectively with $LiCp^N$ (Scheme I). Both compounds were found to be relatively stable to air in the pure state or in benzene or toluene solutions for days, but for polymerizations they should be freshly prepared. We assume that they are analogous in structure to Pd(Cp)(allyl)[56] and $Pt(Cp)Me_3$,[57] respectively. We designed these monomers with several properties in mind: they should not react adversely with the polymerization initiator, the polymer should be soluble enough for film casting, and the metal complexes should decompose readily under mild conditions (thermally, photochemically, or chemically).

Polymer Synthesis. Polymerizations were conducted in toluene using either $Mo(CHCMe_2Ph)(NAr)(O\text{-}t\text{-}Bu)_2$ or $W(CH\text{-}t\text{-}Bu)(NAr)(O\text{-}t\text{-}Bu)_2$ as the initiator. NMR studies showed that both organometallic monomers (15 equiv) are rapidly and quantitatively polymerized by $Mo(CHCMe_2Ph)(NAr)(O\text{-}t\text{-}Bu)_2$ initiator in C_6D_6. The NMR resonances characteristic of metal alkylidene α protons

(50) Cullity, B. C. Elements of X-Ray Diffraction; Addison-Wesley Publishing Co.: Reading, MA, 1978; p 102.
(51) Berney, C. V.; Cheng, P.-L.; Cohen, R. E. *Macromolecules* **1988**, *17*, 2235.
(52) Kinning, J. K.; Thomas, E. L. *Macromolecules* **1984**, *17*, 1712.
(53) Percus, J. K.; Yevick, G. J. *Phys. Rev.* **1958**, *110*, 1.
(54) Wertheim, M. S. *Phys. Rev. Lett.* **1963**, *10*, 321.
(55) Thiele, E. J. *Chem. Phys.* **1963**, *39*, 474.
(56) Shaw, B. L. *Proc. Chem. Soc.* **1960**, 247.
(57) Robinson, S. D.; Shaw, B. L. *J. Chem. Soc.* **1965**, 1529.

Table I. Morphological Characterization of Polymers (Length Scales in angstroms)

polym sample	composition	predicted mol wt	wt % organometallic block	wt % metal atom	morphology	TEM morphological length scale[a]	SAXS interdomain length scale[b] first peak	SAXS interdomain length scale[b] second peak
precursor								
L	$[Pd]_{50}[MTD]_{113}$	39400	50	14	lamellar	170	291	290
C	$[Pt]_{40}[MTD]_{200}$	51200	32	15	cylindrical	220	369	381
S	$[Pd]_{10}[MTD]_{163}$	32400	12.5	3	spherical		212	
posttreatment								
L	$[Pd]_{50}[MTD]_{113}$				lamellar	180	301	294
C	$[Pt]_{40}[MTD]_{200}$				cylindrical	205	349	
S	$[Pd]_{10}[MTD]_{163}$				spherical		203[d]	
$[Pd]_{100}$	$[Pd]_{100}$	39500	100	27				
$[Pt]_{100}$	$[Pt]_{100}$	41000	100	48				

[a] Interdomain distance determined by TEM. [b] Determined from Bragg d spacing. [c] Interdomain distance determined from Percus–Yevick fit. [d] We do not known whether the scattering is from the microdomains or the clusters. [e] Determined from Bessel function fit. [f] Determined from Scherrer's equation. [g] The fit of the Bessel function of the scattering curve was poor due to the bimodal distribution of cluster sizes. [h] Cluster–cluster distance determined from Percus–Yevick fit.

(11.5–11.7 ppm) completely disappeared upon addition of 10 equiv of monomer and were replaced by a resonance at 11.61 ppm, analogous to the alkylidene resonance of living polynorbornene made with the same initiator. Homopolymers of $Pd(Cp^N)(PA)$, $Pt(Cp^N)Me_3$, and MTD will be written as $[Pd]_n$, $[Pt]_n$, and $[MTD]_n$, respectively, where n represents the number of equivalents of monomer used per equivalent of initiator.

$[Pd]_{100}$ and $[Pt]_{100}$ were prepared quantiatively in 15 min and did not precipitate from toluene in the concentration range of ca. 3–5% by weight of polymer. The homopolymers were cleaved from the metal in a Wittig-like reaction by adding excess pivaldehyde. A portion of the reaction solution was removed and examined by NMR after removing solvent and redissolving the residue in C_6D_6; no resonances ascribable to unreacted monomer were present. Films were cast by allowing solutions in polyethylene cups to evaporate slowly in a nitrogen glove box at room temperature over 6–10 days and then kept under high vacuum for at least 24 h. The $[Pd]_{100}$ homopolymer film was hard, brittle, and dark red, the color of the palladium complex, whereas the $[Pt]_{100}$ homopolymer film was soft, transparent, and pale yellow due to trace amounts of $Mo(O)(NAr)(O\text{-}t\text{-}Bu)_2$, the product of the termination reaction with pivaldehyde. (The platinum complex itself is colorless.) Analysis by DSC showed that the $[Pd]_{100}$ homopolymer decomposes above 115 °C with no glass transition being observed, whereas the $[Pt]_{100}$ homopolymer exhibits a glass transition at 30 °C and is stable up to 150 °C.

Samples of $[Pd]_{50}$ and $[Pt]_{55}$ homopolymers (synthesized as described above) were examined by GPC; the $[Pd]_{50}$ homopolymer had a polydispersity index, X_n, of 1.16 and a polystyrene-equivalent number average molecular weight (M_n) of 22500 (calcd M_n = 19700) whereas the $[Pt]_{55}$ homopolymer had a X_n of 1.13 and M_n of 17400 (calcd M_n = 22600). (A conversion factor between the actual organometallic polymer M_n and polystyrene M_n is not known.) Both the GPC and the NMR results suggested that the metal-containing monomers are ring-opened in a well-behaved, living manner.

Diblock copolymers S, C, and L (see Table I) were synthesized by sequentially adding MTD and the appropriate organometallic monomer to the alkylidene initiator, as outlined in Scheme II. (A typical procedure is given in the Experimental Section.) After the polymerization of MTD, a weighed fraction of the solution (usually one-third) was removed and treated with excess pivaldehyde. GPC analysis of $[MTD]_{113}$, $[MTD]_{163}$, and $[MTD]_{200}$ gave polydispersities of 1.07, 1.05, and 1.04 with average polystyrene-equivalent molecular weights of 23200, 32300, and 41800, respectively. An appropriate amount of the metal-containing monomer was then added to the living polyMTD to form the diblock. After termination, the Pd- or Pt-containing block copolymers were precipitated in pentane or in methanol, respectively, in order to remove $Mo(O)(NAr)(O\text{-}t\text{-}Bu)_2$. The copolymers were then analyzed by ^1H NMR. In all cases the yields were quantitative and the NMR data were consistent with the targeted diblock. The diblocks were dissolved in benzene (3 wt %), and 0.3–0.5-mm thick hard, stiff films were cast. The films containing palladium are dark red, and those containing platinum are pale yellow.

Scheme II. Sequential Polymerization of MTD and the Metal-Containing Norbornene Derivative

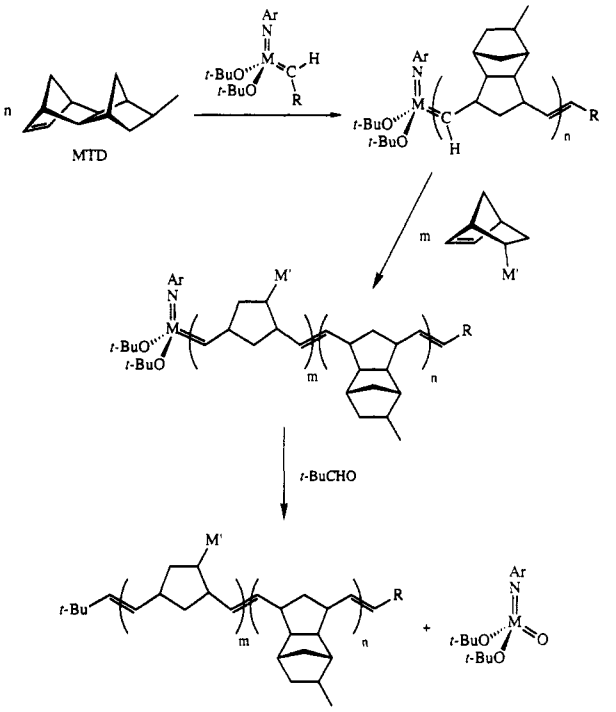

M = Mo, W; Ar = 2,6-C_6H_3-i-Pr_2; R = t-Bu, CMe_2Ph; M' = $CH_2CpPd(PA)$, $CH_2CpPtMe_3$

Cluster Formation. The $Pd(Cp^N)(PA)$ monomer reacted with H_2 (1 bar) at room temperature within minutes both in solution and in the solid state to give palladium metal cleanly and liberate the reduced ligands (Scheme III). However, the palladium-containing polymer films had to be heated to 100 °C under a hydrogen pressure of 5 bar for at least 3 days to ensure complete reaction. Monitoring

SAXS hard-sphere diam[c]	TEM diam of microdomain	SAXS diam of microdomain[e]	WAXS cryst size of clusters[f]	TEM cluster diam	SAXS diam clusters[e]	SAXS cluster–cluster length scale[b]	SAXS cluster hard-sphere diam[h]
	70						
	65						
216	25	96					
			21–25	20–40			
			24–27	30–50	72	193	170
195[d]		70[d]	24	20–40		203[d]	193[d]
			27–67	25–120	*g*	101	80
				50–120			

of the reaction by WAXS (bulk sample) and TEM (thin section cut from the bulk sample after treatment) showed that cluster formation was virtually complete after a day and that neither cluster size nor size distribution changed noticeably thereafter.

Preliminary tests showed that the $Pt(Cp^N)Me_3$ complex does not react with H_2 at room temperature. An analogous complex, $Pt(Cp)Me_3$,[58] has been reported to decompose to platinum metal in solution when exposed to UV light in the presence of air via brown intermediates that were not identified. We assumed that the brown intermediates contained Pt(II) and therefore were likely to react more readily with hydrogen. Exposure of the Pt-containing polymer films to UV light for 24 h caused the color to change from pale yellow to dark brown. After UV exposure, WAXS analysis of the brown film showed no diffraction due to platinum metal. The brown film was subsequently treated with H_2 (4 bar) at 100 °C for 3 days, during which time it turned black. At this point, platinum clusters were observed by WAXS, TEM, and ED.

Morphology of Precursor Polymers. A summary of the morphological characterization for each of the polymers is presented in Table I. The TEM micrograph of polymer S had poor contrast and revealed only a scattering of dark, ~25-Å spots (Figure 1a). These spots did not clearly indicate microphase separation. However, the SAXS profile for S was consistent with microphase separation. The scattering profile was a broad ring and lacked higher order Bragg reflection peaks observed in ordered systems containing spherical microdomains. The Percus-Yevick/Bessel function scattering model fit the radially averaged SAXS profile well and was very sensitive to microdomain size, as seen in Figure 1c.

The static cast film of polymer C had a cylindrical morphology with short-range hexagonal packing of the metal-containing block (Figure 2a). In the TEM micrograph, the metal-containing microdomains appear as darker regions. The two-dimensional X-ray scattering profile (Figure 2c) exhibited two rings, indicative of a locally well-ordered, macroscopically unoriented morphology in agreement with TEM analysis. The rings corresponded to two Bragg interference reflections with reciprocal spacings in the ratio $1:3^{1/2}$. This ratio is proof of a hexagonally close-packed cylindrical morphology.[59]

The film of polymer L exhibited lamellar morphology (Figure 3a), as expected for a block copolymer that contains ~50% by weight a metal-containing block. The SAXS profile for L (Figure 3c) also had two peaks, corresponding to the first- and second-order Bragg reflections. The reciprocal spacings of these reflections were in the ratio 1:2, indicative of a lamellar morphology. As for film C, the sample displays a locally well-oriented morphology.

Morphology of Homopolymers after Reduction. The TEM micrograph of the $[Pd]_{100}$ (Figure 4) showed metal clusters in the film with a bimodal size distribution in the range 25–40 Å and some in the range 80–120 Å. Larger clusters appeared to be aggregates of smaller clusters. The SAXS profile of the sample (not shown here) had a relatively broad ring, indicative of an unorganized, phase-separated system containing a distribution of *d* spacings. Crystal sizes of 67 and 27 Å were determined from the [111] and the [220] peaks, respectively, of the WAXS profile.

Clusters also were prepared within the $[Pt]_{100}$ homopolymer, as seen in the TEM micrograph in Figure 5. Originally the film was soft and pale yellow. After 24 h under UV light the film had changed to a hard, brittle, brown solid. The brown film was then treated with hydrogen, as described in the Experimental Section, to give a very brittle, black solid. The TEM (the brittle polymer was embedded in epoxy to facilitate microtoming) revealed clusters in the range 50–120 Å in diameter. There appeared to be more cluster aggregation than in the $[Pd]_{100}$ film. Moreover, the clusters were not dispersed homogeneously throughout the $[Pt]_{100}$ film; the micrograph showed large areas of polymer in which clusters were absent. Analysis of $[Pt]_{100}$ by SAXS did not provide any conclusive information on the nature of the clusters in the film.

Morphology of Diblock Copolymers after Reduction. Reduction of sample S with hydrogen and heat resulted in the morphology shown in Figure 1b. The presence of Pd clusters, seen as dark spots in the TEM, was readily apparent. Unlike the clusters in the homopolymer films (Figures 4 and 5), these clusters were homogeneously dispersed within the matrix and had a narrow size distribution in the 20–40-Å range. The SAXS profile consisted of a ring that was not nearly as broad as in the scattering profiles of the postreduction homopolymers. The Percus–Yevick/Bessel function model fit the scattering profile for a sphere diameter smaller than that determined for the same sample before the treatment. However, it could not be determined whether the ring in the profile was due to the spherical microdomains or the palladium clusters. Only the diffraction peak of the [111] plane in the palladium fcc crystal was visible in the WAXS profile of the film. A crystal size of 24 Å was determined from this peak.

(58) Hackelberg, O.; Wojcicki, A. *Inorg. Chim. Acta.* **1980**, *44*, L63.
(59) Hadziioannou, G.; Skoulios, A. *Macromolecules* **1982**, *15*, 267.

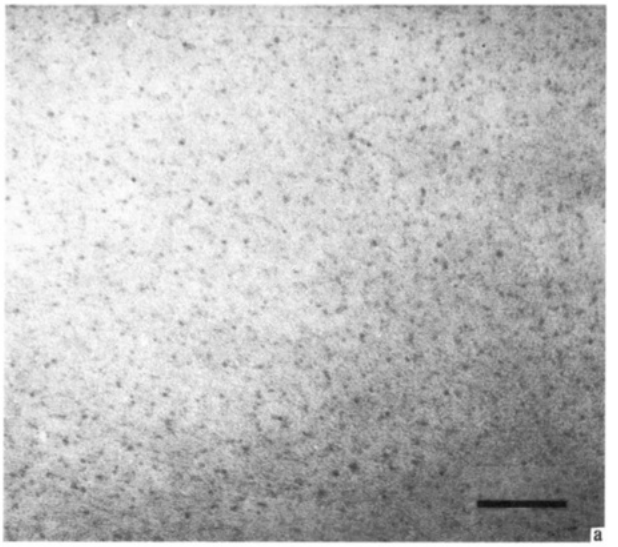

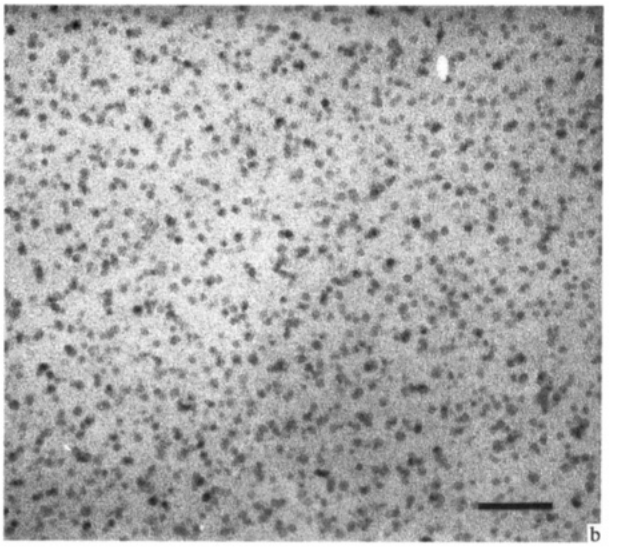

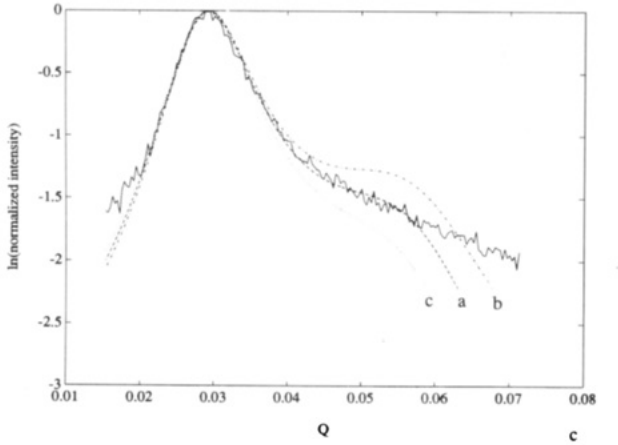

Figure 1. (a) Electron micrograph of S before reduction (bar = 500 Å). (b) Electron micrograph of S after reduction (bar = 500 Å). (c) SAXS scan of S before reduction. Fits of Percus–Yevick/Bessel function model of scattering shown as dashed lines. Curves a, b, and c used input intraparticle radii of 48, 43, and 53 Å, respectively. Interparticle interference parameters were identical in the three cases. Plot is in the form of normalized log of radial-averaged intensity (counts) vs the scattering vector Q ($Å^{-1}$).

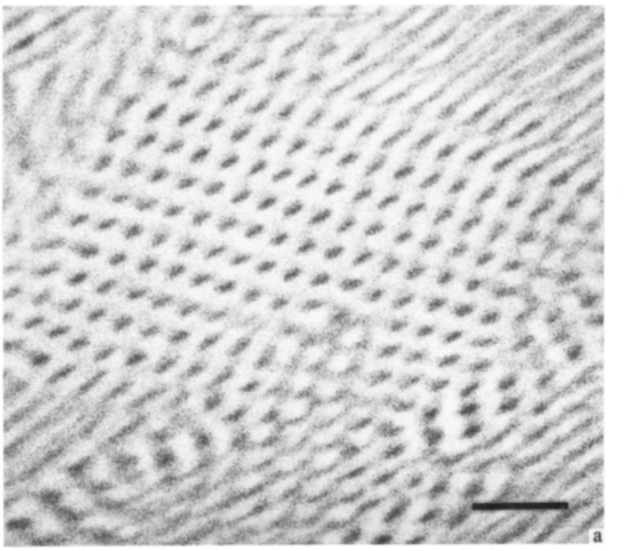

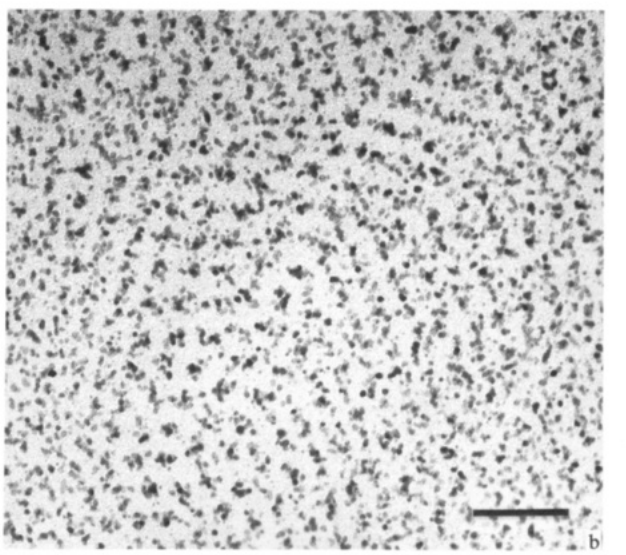

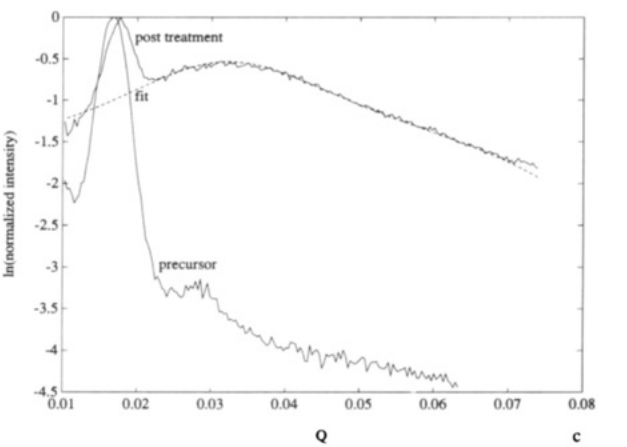

Figure 2. (a) Electron micrograph of C before reduction (bar = 750 Å). (b) Electron micrograph of C after reduction (bar = 750 Å). (c) Radial-averaged SAXS scans of C before and after reduction.

The TEM of a thin section of polymer C after the UV/H_2 treatment is shown in Figure 2b. Clusters ranging in size from 30 to 50 Å were formed preferentially within the original metal-containing microdomains. The original cylindrical morphology of the precursor polymer was still noticeable. The SAXS profile of reduced C is shown in Figure 2. The first-order Bragg reflection, associated with the spacing of the cylindrical features of the morphology, was identical in both the precursor and reduced films. However, in the profile of the reduced film a broad, high-intensity peak at large scattering angle was present. This broad peak apparently was caused by the cluster–

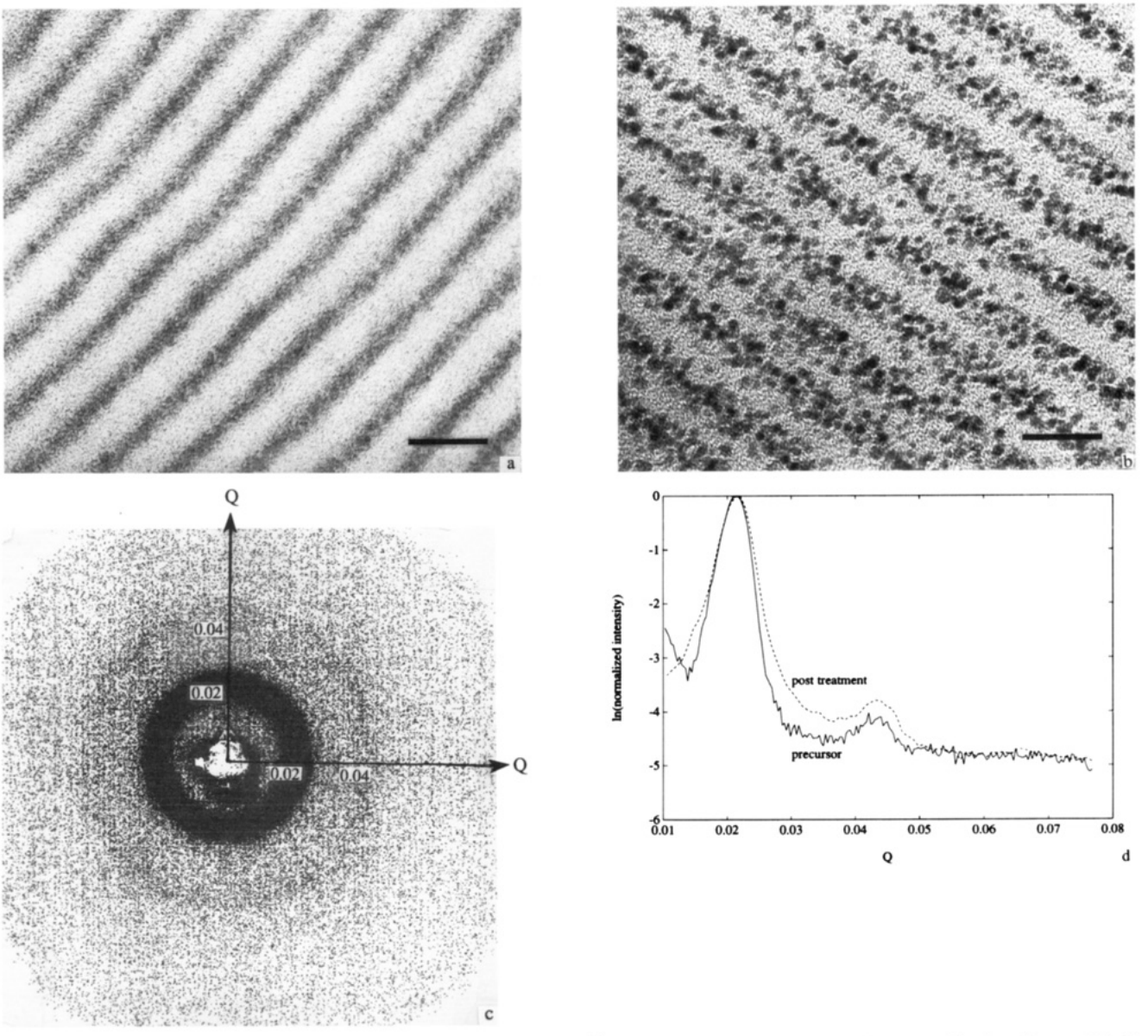

Figure 3. (a) Electron micrograph of L before reduction (bar = 250 Å). (b) Electron micrograph of L after reduction (bar = 250 Å). (c) Two-dimensional SAXS profile of L before reduction. (d) Radial-averaged SAXS scans of L before and after reduction.

cluster *d* spacings within the cylindrical microdomains. The *d* spacing corresponding to the peak location was much smaller than the *d* spacing of the cylindrical microdoamins, and the breadth of peak was indicative of a broad distribution of *d* spacings.

The progression of WAXS profiles for sample C from the precursor film to the cluster-containing composite appears in Figure 6. The broad band at about $2\theta = 16°$ was caused by scattering from the amorphous polymer matrix. Peaks caused by the clusters appear at larger values of 2θ. There was no evidence of cluster formation in the precursor film or after exposure to UV light. Clusters were observable only after heating the sample under H_2. The final profile contained peaks characteristic of the [111], [200], [220], and [311] crystallographic planes of platinum metal (fcc). Average crystal sizes estimated from different peaks of the WAXS profile were 24–27 Å.

Treatment of sample L with hydrogen for 6 days resulted in the formation of palladium clusters that ranged in size from 20 to 40 Å, as seen in Figure 3b. As in the preceding case, the original morphology was retained, clearly suggesting that majority of the clusters formed within the metal-containing microdomains of the film. However, some of the clusters appeared to be located outside the lamellae that originally contained the metal complex. Unlike film C, the radial-averaged SAXS profile of L, Figure 4d, did not contain a peak due to clusters. Instead, the profile appeared to be very similar to the film before reduction. It consisted of two Bragg reflections arising from the initial lamellar morphology. The interdomain spacing found from SAXS had not changed after reduction. Analysis by WAXS gave diffraction patterns characteristic of palladium metal with peaks due to the [111], [200], and [220] planes of the fcc lattice (Figure 7). Crystal sizes determined from each of the three different crystalline peaks of the WAXS profile were in the range 21–25 Å. The polycrystalline and metallic nature of the clusters was also evident from electron diffraction studies.

Discussion

Cluster Formation. In the electron micrographs of the L (Figure 3b) and C (Figure 2b) films after treatment, it is clear that the metal clusters formed largely within the original metal-containing microdomains. But the fact that some of the clusters are found outside the microdomains suggest that metal atoms or small clusters can travel

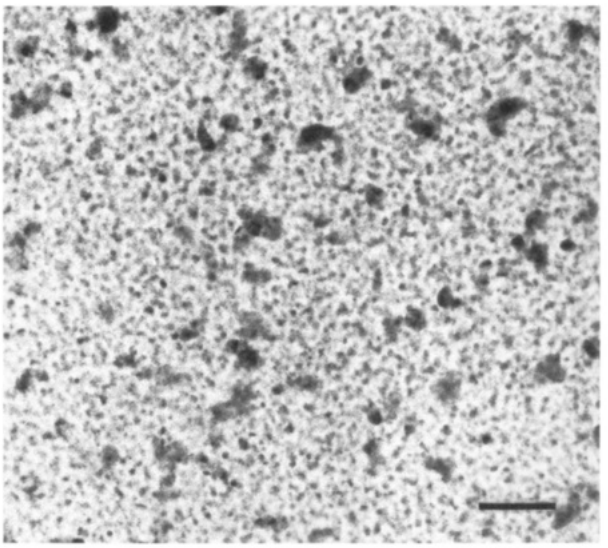

Figure 4. Electron micrograph of $[Pd]_{100}$ after reduction (bar = 500 Å).

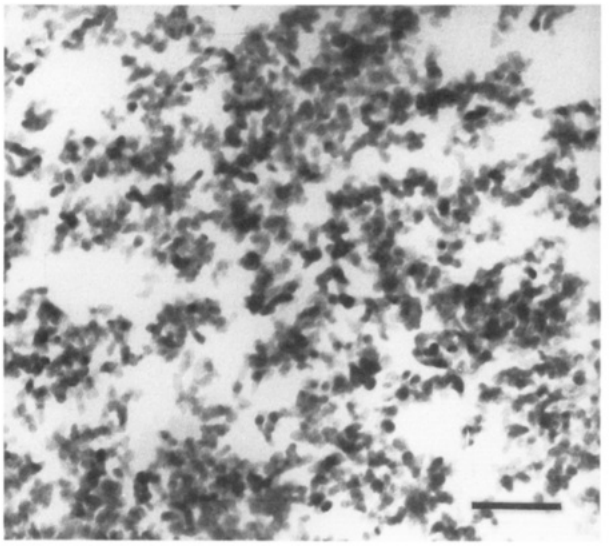

Figure 5. Electron micrograph of $[Pt]_{100}$ after reduction (bar = 500 Å).

through the polymer before creating or reaching a nucleation site. The mobility of atoms or small clusters within the polymer matrix is surprising considering the high T_g (210 °C) of polyMTD, a temperature well above that at which clusters were generated. Carbon–carbon double bonds could assist this process, but they are likely to be hydrogenated to a significant extent within the metal-containing microdomain subsequent to formation of reduced metal. It is also worthwhile to consider the possibility that diffusion of metal atoms and clusters could be enhanced by localized heating and volume changes in the material caused by the exothermic reduction process. The formation of and location of the metal clusters should depend on the relative rate of creation of nucleation sites versus the rate of cluster growth and the mobility of the atoms or clusters. The narrow distribution of cluster sizes observed might be ascribed to a reduced mobility of clusters whose size is >20 Å. The local concentration of metal complex effectively limits cluster size by controlling the number of metal atoms available given a fixed number of nucleation sites. Also, it seems likely that the fusion of two or more metal clusters beyond a certain size is not kinetically favored under the conditions used. A higher temperature would be required for this process, although

Scheme III

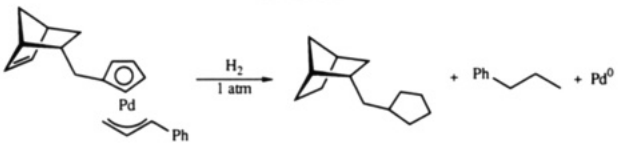

treating film L at 160 °C instead of 100 °C produced the same result according to TEM.

In the case of the S polymer film, for which we assume a spherical morphology with domain size of about 25 Å as estimated by TEM and 96 Å by SAXS (see below), the clusters obtained after treatment were in the range 20–40 Å, as estimated by TEM. We note that the clusters in the S film are in the same range as in the L film although the metal content is 4 times greater in the latter film. Whether atoms or clusters migrated between domains is not clear at this point because of the uncertainty in estimating the original metal-containing domain size.

In contrast, the clusters that were formed within the Pd- and the Pt-containing homopolymers have a much wider distribution of sizes. This could be the consequence of the high metal content (Table I) of the polymer films. Originally the weight fraction of metal in the $[Pd]_{100}$ film is about 27%, but after treatment this ratio can increase to 38% as the phenylallyl ligand is reduced to the volatile *n*-propylbenzene (Scheme III). However, removal of the reduced ligand could be incomplete even at 100 °C because chemisorption on the metal surface is possible. For the $[Pt]_{100}$ homopolymer film the metal content before treatment is 41%. After treatment this value is also higher due to loss of hydrocarbon gases[58] (mostly methane), although the decomposition mechanism is not known. One could argue that the local concentration of metal precursors should be the same in the homopolymer and in the microdomains of the diblock copolymers, and this should result in the same cluster size distribution. However, the confinement in one or more dimensions restrict the cluster growth by decreasing the total amount of metal atoms available per nucleation site. We note also in the micrograph of Figure 5, the $[Pt]_{100}$ homopolymer film after treatment, that there is much more aggregation than in the case of the $[Pd]_{100}$ homopolymer film (Figure 4).

It is also possible that the difference in cluster sizes observed in the homopolymer and copolymer films is related to the structure of the polymers. In the microphase-separated systems, the polymer chains within the microdomains lack mobility because of chain junctions at the microdomain interface and because of the constrained volume of the microdomains. The mobility of homopolymer chains is not restricted in this manner, and the homopolymer therefore could allow large metal particles to migrate and grow.

Characterization of Polymer and Cluster Morphologies. There is a significant discrepancy between the morphological length scales determined by SAXS and by TEM, as seen in Table I. This discrepancy has been observed previously in purely organic block copolymers, and potential causes have been discussed in the literature.[60] For example, the polymer sample undergoes a large amount of compression and shear during the microtoming process before being examined by TEM, whereas bulk material has been used to obtain SAXS data. However, the trends observed from TEM micrographs were consistent with those observed from SAXS data. In samples L and C, the ratios of the reciprocal spacings of the first

(60) Berney, C. V.; Cohen, R. E.; Bates, F. S. *Polymer* **1982**, *23*, 1222.

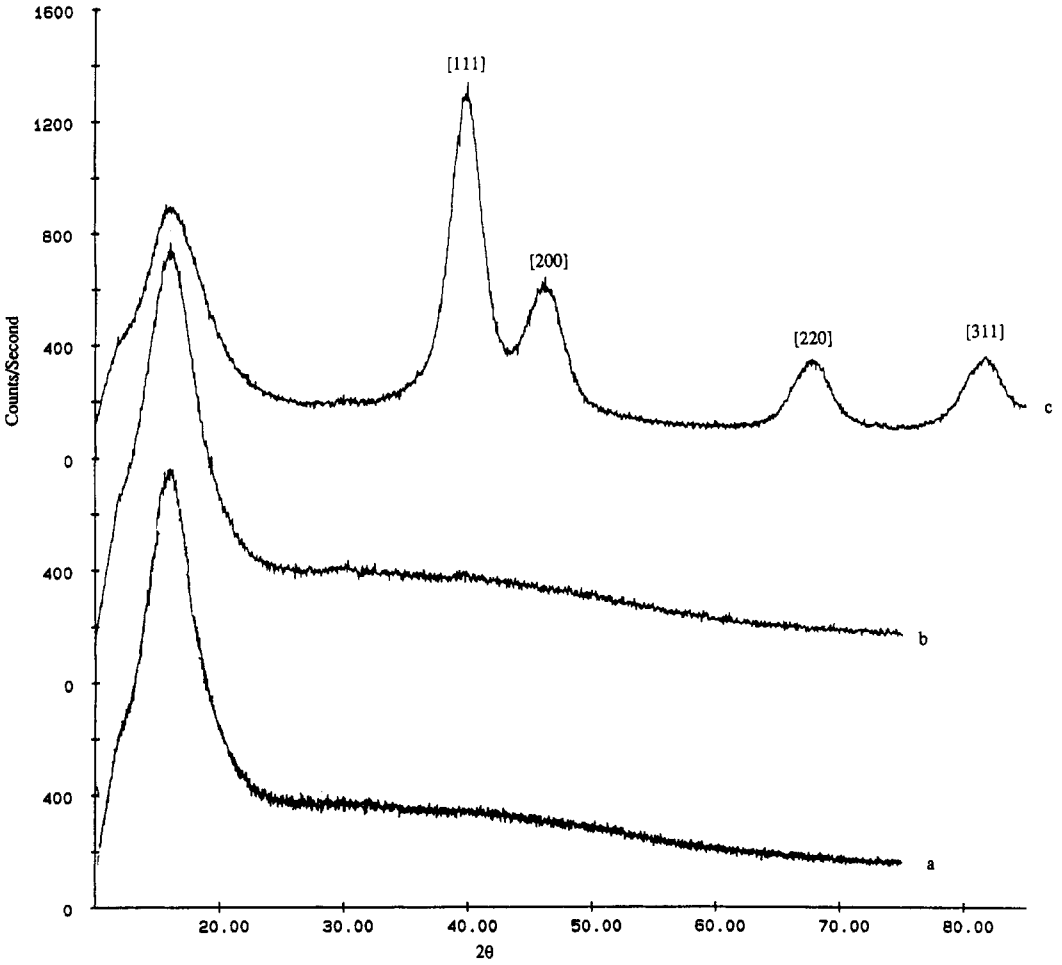

Figure 6. WAXS profiles of C: (a) before reduction; (b) after exposure to UV light for 24 h; (c) after subsequent exposure to H_2 (5 bar) at 100 °C for 3 days. Scattering curves are offset for sake of comparison. Numbers in brackets refer to the Pt crystallographic plane associated with the scattering peak.

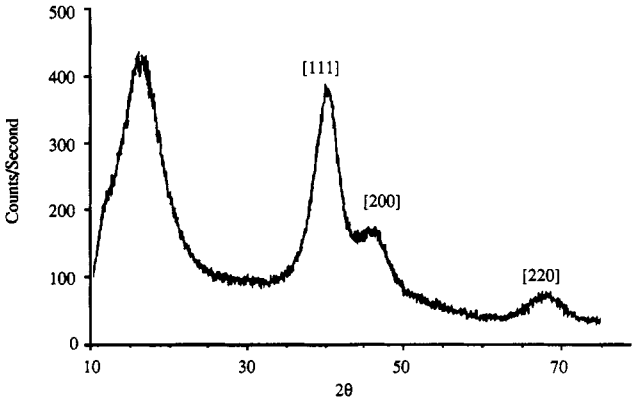

Figure 7. WAXS profile of L after exposure to H_2 (5 bar) at 100 °C for 6 days. Numbers in brackets refer to the Pd crystallographic plane associated with the scattering peak.

and second Bragg reflections indicated unambiguously the type of morphology within the sample. In the case of sample S, the good fit of the SAXS profile with the Percus–Yevick model, along with the absence of higher order Bragg reflections, led to the conclusion that it was a disordered spherical morphology.

We have one reservation regarding the use of the Percus–Yevick/Bessel function formulation for modeling the SAXS profiles of spherical or cluster-containing morphologies. For the Bessel function form factor to be applied with complete certainty, a distinct shoulder must be present in the radial-averaged profile. The profiles presented here lack such a distinct shoulder. In the profile for film S shown in Figure 1c, it was possible that the scattering at larger values of the scattering vector Q was caused by residual background scattering and not intraparticle scattering. If that were the case, the use of the Bessel function form factor would provide information on the minimum size of the spheres in sample S. As seen in the fits in Figure 2c, smaller input values for the sphere radius would result in a higher intensity of scattering at large Q values.

The Percus–Yevick/Bessel function model did fit the scattering profile of S before and after reduction. However, we were unable to determine whether the SAXS pattern after reduction was caused by the extant spherical microdomains or the newly formed clusters. It is interesting to note that a peak associated with the clusters in the SAXS profile of C was present after treatment but not in the profile of L after treatment. The absence of a peak due to clusters could have resulted from a very broad distribution of cluster–cluster d spacings within L. Attempts to fit the Bessel function model to the scattering profiles of the homopolymers were unsuccessful, presumably because the model does not hold for a very broad distribution of cluster sizes. The Percus–Yevick formulation could still be used to determine the interparticle distance in $[Pd]_{100}$.

Line-broadening analysis of WAXS peaks using Scherrer's equation yields crystallite size of a material, not necessarily cluster size. If the clusters were polycrystalline, the size determined from Scherrer's equation should be smaller than that from either SAXS or TEM. Clusters observed in TEM may have been disrupted or deformed

during the microtoming process. The results from TEM and WAXS, however, are in good agreement, notably in the case of diblock copolymers where narrow distribution of cluster sizes were observed. By SAXS, the Bessel function fit of the profile may only provide a lower bound on cluster size, analogous to the fit of the spherical microdomains in sample S. We found that the cluster size estimated by this technique for sample C was actually bigger compared to the size estimated by TEM (Table I). In the case of the homopolymers, a fit of the Percus-Yevick/Bessel function formulation could not be obtained.

As mentioned in the Introduction, it is desirable to have a uniform distribution of clusters in the composite material. Whether or not the clusters formed in the block copolymers could be said to be "uniformly distributed" depends upon the length scale examined. Within the microdomains, the clusters appeared to be uniformly, albeit randomly, distributed. However, as the length scale of consideration is increased to the d spacing of the material, the cluster distribution would have the form of a step function and not a uniform distribution. As the length scale is increased to bulk dimensions, inhomogeneities seen in the microdomains are averaged out by the various orientations of sections of the microdomains. It would be interesting to obtain samples with macroscopically well-ordered metal cluster-containing cylindrical or lamellar morphology since they would display anisotropic properties.

Conclusion

The two organometallic monomers presented herein provide a relatively straightforward method of synthesizing palladium and platinum nanoclusters within a nonconductive polymeric matrix. They cleanly undergo ROMP with a well-defined metal alkylidene initiator to give homopolymers or diblock copolymers with the desired composition that are stable and tractable. The block copolymers exhibit microphase separation with morphologies that are consistent with their compositions. Reduction of the metal complexes in the solid polymer films under relatively mild conditions affords clusters in the range 20–125 Å in diameter (a size which depends on the nature of the polymer) that are metallic in nature, according to X-ray studies. The microphase-separated morphology of the block copolymers provided enhanced kinetic control of the cluster formation process, effectively eliminating cluster aggregation into larger particles observed in the reduced organometallic homopolymers. Extended heating of cluster-containing films did not result in excessive aggregation of these small clusters. Further syntheses and annealing studies are planned in order to explore this kinetic limitation.

The diblock approach is effective if small clusters with a narrow size distribution are desired. The small dimensions of the metal-containing microdomains appear to limit cluster size. The studies reported here should be compared with related studies concerning the preparation of gold and silver clusters in block copolymers.[38] It also now seems possible to grow a single cluster within a spherical microdomain, the ultimate control in cluster growth and size.[61] Research to examine the dielectric and nonlinear optical properties of these cluster-containing composite materials is in progress.

Acknowledgment. We thank the National Science Foundation (Grant DMR 87-19217 through the MIT Center for Material Science and Engineering) and Nippon-Zeon for financial support. The B.F. Goodrich Co. is acknowledged for a generous supply of MTD. Helpful discussions with C. C. Cummins and a gift of $Li(Cp^N)$ from him are appreciated. G.S.W.C. acknowledges the NSF for a Graduate Fellowship.

Registry No. $Mo(CHCMe_2Ph)(NAr)(O\text{-}t\text{-}Bu)_2$, 126949-65-3; $W(CH\text{-}t\text{-}Bu)(NAr)(O\text{-}t\text{-}Bu)_2$, 107440-84-6; $Pd(Cp^N)(PA)$, 141483-81-0; $LiCp^N$, 141485-36-1; $[Pd(PA)Cl]_2$, 12131-44-1; $Pt(Cp^N)Me_3$, 141483-86-5; $[PtMe_3I]_4$, 18253-26-4; $[Pd(Cp^N)(PA)]_n$, 141483-82-1; $[Pt(Cp^N)Me_3]n$, 141483-84-3; [Pd]50[MTD]113, 141483-85-4; [Pt]40[MTD]200, 141483-87-6.

(61) Ng Cheong Chan, Y., unpublished results.

Protonated Pentatitanate: Preparation, Characterizations, and Cation Intercalation

Takayoshi Sasaki,* Yu Komatsu, and Yoshinori Fujiki

National Institute for Research in Inorganic Materials, 1-1 Namiki, Tsukuba, Ibaraki 305, Japan

Received March 3, 1992. Revised Manuscript Received May 18, 1992

A protonated pentatitanate with a monoclinic layer structure, $H_2Ti_5O_{11}\cdot 3H_2O$, has been prepared by treating its parent compound, $Cs_2Ti_5O_{11}$, with a hydrochloric acid solution. The hydration water, as well as protons, is introduced upon interlayer Cs ion removal, expanding the separation between lost lamellae, $[Ti_5O_{11}^{2-}]_\infty$. Half of the substituting protons exist as oxonium ions and the other half as hydroxyl groups, both of which are reversibly exchangeable with cations. The material lost free interlayer water up to 100 °C yielding a less hydrated phase, $H_2Ti_5O_{11}\cdot H_2O$, with a smaller interlayer distance. Subsequent dehydration resulted in the metastable form of titanium dioxide TiO_2(B) around 500 °C, which was transformed into anatase and then rutile at elevated temperatures. The material $H_2Ti_5O_{11}\cdot 3H_2O$ underwent a stepwise intercalation reaction with K and Cs ions, replacing oxonium ions and hydroxylated protons in this order. This reaction gave rise to half- and fully-loaded phases with different degrees of swelling. The structural characterizations of the phases indicate that the reaction proceeds topochemically, accompanied by a lateral gliding of adjacent host lamellae along the c axis as well as a swelling/contraction of the interlayer spacing.

Introduction

There are a series of layered titanates with the general formula $M_2O\cdot nTiO_2$ (where M denotes alkali-metal ions). The crystal structures are composed of host lamellae and charge-compensating interlayer cations, as shown schematically in Figure 1. The following members are ca-

0897-4756/92/2804-0894$03.00/0